

Electronic Supplementary Information (ESI) for:

Elucidating the relationship between nanoparticle morphology, nuclear/magnetic texture and magnetic performance of sintered $\text{SrFe}_{12}\text{O}_{19}$ magnets.

Matilde Saura-Múzquiz,^{*a,b,†} Anna Zink Eikeland,^a Marian Stingaciu,^a Henrik Lyder Andersen,^{a,*} Cecilia Granados-Miralles,^{a,‡} Maxim Avdeev,^b Vladimir Luzin^b and Mogens Christensen^{*a}

^a Center for Materials Crystallography, Department of Chemistry and iNANO, Aarhus University Langelandsgade 140, DK-8000 Aarhus C, Denmark

^b Australian Nuclear Science and Technology Organisation (ANSTO), New Illawarra Road, Lucas Heights NSW 2234 Australia

[†] Current address: School of Chemistry, University of Sydney, F11, Sydney, NSW 2006, Australia

^{*} Current address: School of Chemistry, The University of New South Wales, Sydney, NSW, 2052, Australia

[‡] Current address: Electroceramics Department, Instituto de Cerámica y Vidrio, CSIC, Kelsen 5, ES 28049 Madrid, Spain

**Corresponding authors:*

M.S.M.: matilde.saura@sydney.edu.au

M.C.: mch@chem.au.dk

Contents

Spark Plasma Sintering	2
Unit Cell Parameters powder samples.....	3
Rietveld refinements of NPD and PXRD data of powder samples and crushed SPS pellets.....	4
Overview of refined structural parameters of powder samples	4
Sol-Gel (SG)	5
Modified Sol-Gel (MSG)	6
Supercritical Continuous Flow (FL)	7
Autoclave (AC)	9
Overview of refined structural parameters of SPS samples	10
SPS_SG	11
SPS_MSG.....	12
SPS_FL.....	13
SPS_AC.....	14
Refined magnetic moments.....	15
Transmission Electron Microscopy	16
Sol-Gel (SG)	16
Autoclave (AC)	17
Neutron Pole Figures of SPS samples	18
SPS_SG	18
SPS_MSG.....	18

SPS_FL.....	19
SPS_AC.....	19
Crystallite growth with SPS.....	20

Spark Plasma Sintering

The sintering conditions employed for the preparation of the SPS pellets are given in Figure S1.

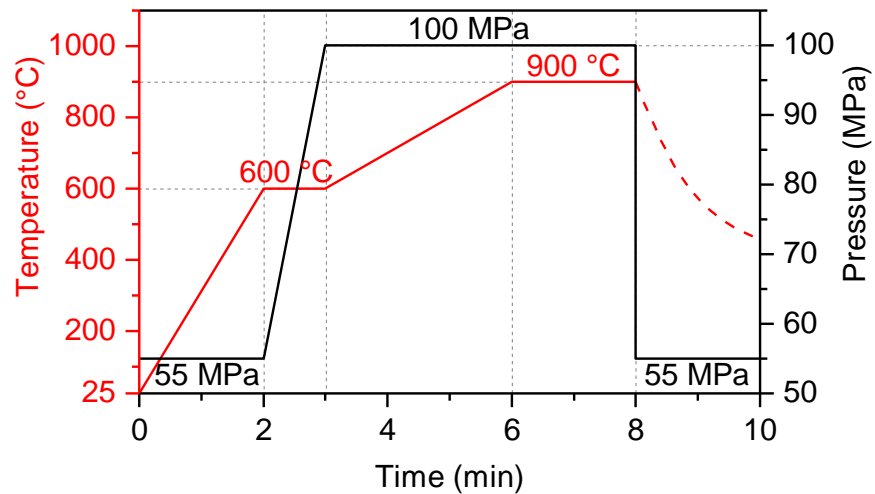


Figure S1: Temperature (red) and pressure (black) employed in the spark plasma sintering of the studied samples.

Unit Cell Parameters powder samples

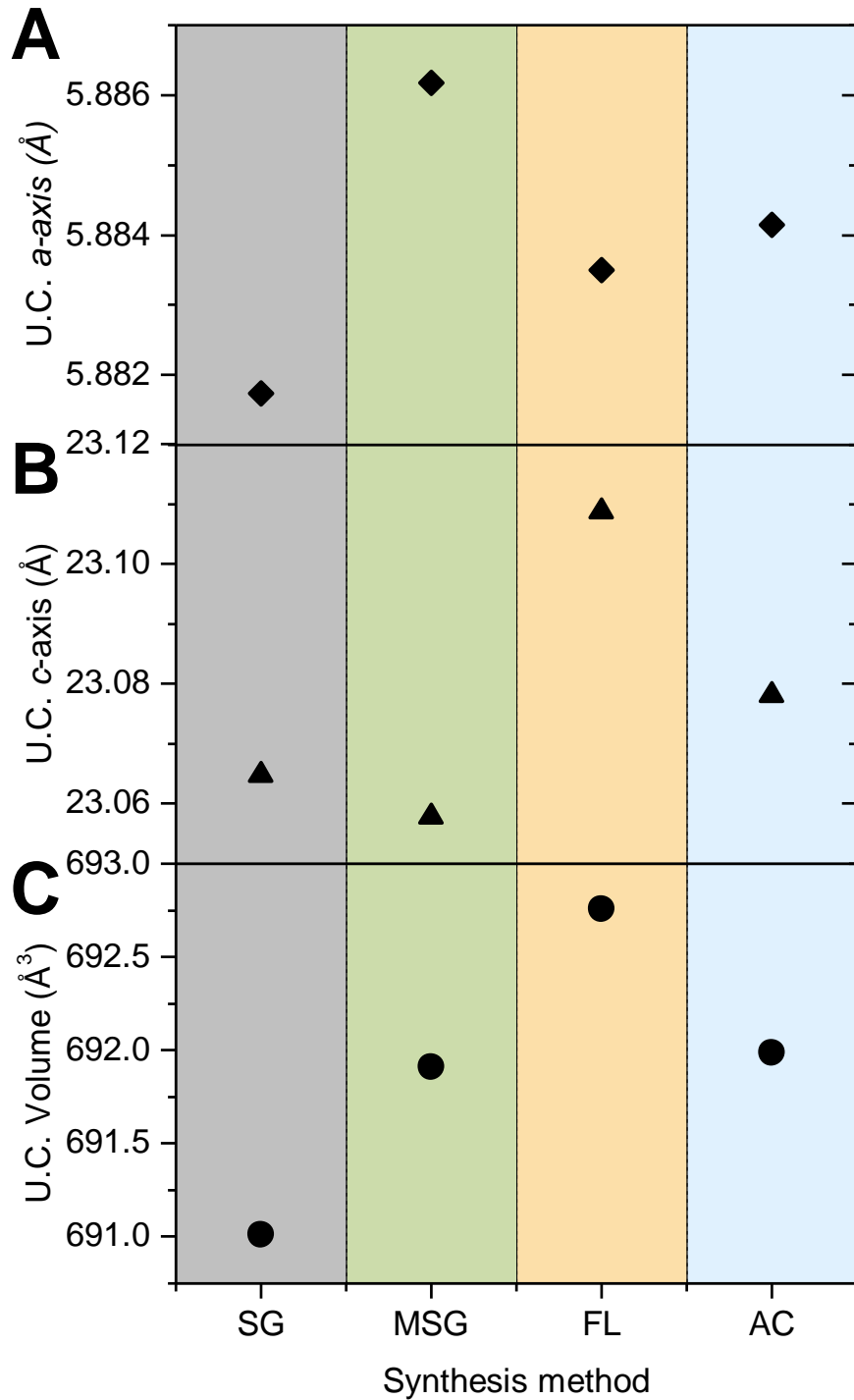


Figure S2: A) Unit cell a -axis, B) unit cell c -axis and C) unit cell volume extracted from the constrained Rietveld refinement of the NPD and PXRD data, for the four as-synthesized samples. The errors lie within the size of the symbols.

Rietveld refinements of NPD and PXRD data of powder samples and crushed SPS pellets

Overview of refined structural parameters of powder samples

Table S1: Extensive summary of the constrained NPD and PXRD refinements including the refined crystal structure and magnetic structure parameters, R-values,etc. (SFO=SrFe₁₂O₁₉)

	SG	MSG	FL			AC
Phases	SFO	SFO	SFO-Small	SFO-Large	FeOOH	SFO
Composition and microstructure:						
Wt%, (%)	100.0(4)	100.0(2)	45.37(2)	25.47(1)	29.16(1)	100.0(5)
Cryst. size, D_a (nm)	73.5(5)	60.1(2)	30.9(4)	130(2)	24.2(7)	98.1(9)
Cryst. size, D_c (nm)	63(1)	23.91(9)	2.80(3)	29.5(3)	7.1(2)	38.3(4)
Crystal structure:						
Space group	$P6_3/mmc$	$P6_3/mmc$	$P6_3/mmc$	$P-31c$	$P6_3/mmc$	
Lattice par., a (Å)	5.88187(3)	5.88624(2)	5.88350(4)	2.94175(8)	5.88433(6)	
Lattice par., c (Å)	23.0654(2)	23.0584(1)	23.1087(3)	9.3154(8)	23.0787(2)	
Cell vol., V (Å ³)	691.07(1)	691.888(6)	692.75(1)	69.814(7)	691.99(2)	
B_{overall} (PXRD/NPD)	-	1.55(1)/0.25(7)	1.99(2)/0.63(5)		1.46(2)/0.14(6)	
B_{iso} (Sr ²⁺)	1.77(6)	-	-	-	-	-
B_{iso} (Fe ³⁺)	1.60(3)	-	-	-	-	-
B_{iso} (O ²⁻)	1.13(4)	-	-	-	-	-
Site occ. Fractions FeOOH:						
Fe ³⁺	-	-	-	0.1313(8)	-	-
Magnetic structure:						
Easy-axis*	<001>	<001>	<001>	-	<001>	
μ_{Fe1Oh} (μ_B)	3.6(2)	3.9(2)	3.7(7)	-	3.6(2)	
μ_{Fe2Oh} (μ_B)	3.00(8)	3.34(9)	3.6(2)	-	3.42(8)	
μ_{Fe3Oh} (μ_B)	-3.38(9)	-3.6(1)	-4.3(3)	-	-3.6(1)	
μ_{Fe4td} (μ_B)	-3.8(1)	-4.1(2)	-2.4(4)	-	-4.2(1)	
μ_{Fe5BP} (μ_B)	3.3(2)	2.9(2)	1.0(7)	-	3.4(2)	
Fit quality:						
R_{Bragg} (%)	5.01/7.22	3.48/3.16	3.26/5.39	4.46/7.55	5.61/6.24	3.92/4.97
R_F (%)	6.79/4.72	3.67/2.56	2.59/3.10	4.14/4.69	3.78/2.70	3.02/3.78
R_{magnetic} (%)	-/6.23	-/4.00	-/4.29	-/5.28	-	-/5.31
χ^2_{global}	7.45	2.55	4.98		1.71	
Data						
Wavelength, (Å)	$\lambda_1 = 1.78919, \lambda_2 = 1.79310/2.43971$					
Background par.	6/2	10/6	10/6		8/2	
Ref. param. (total)	34	42	49		40	
Data points	10501/3225	10501/3149	10501/3149		10501/3149	
Reflect.	168/105	171/105	179/105	27/18	167/105	

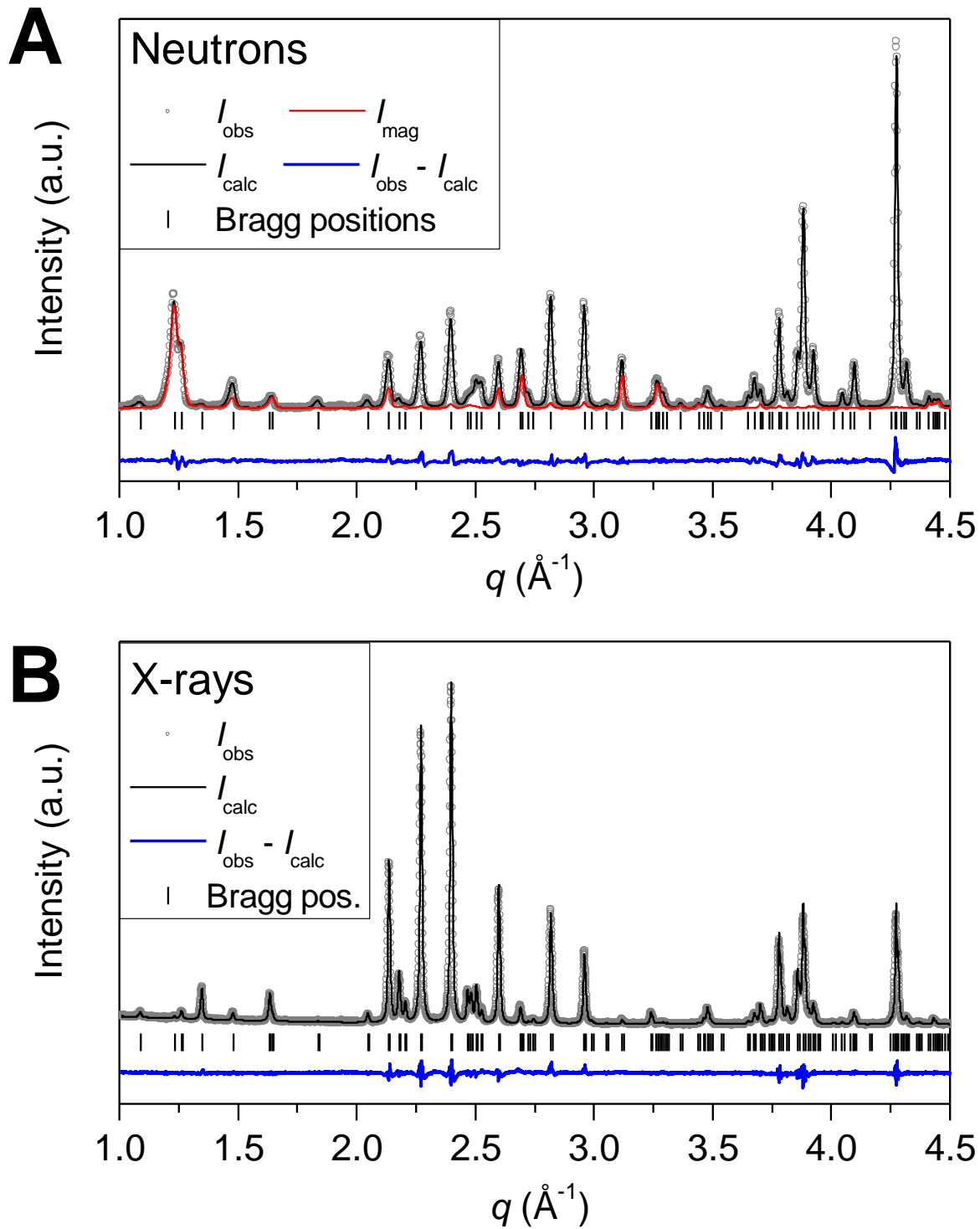


Figure S3: A) NPD and B) PXRD data and constrained Rietveld refinement

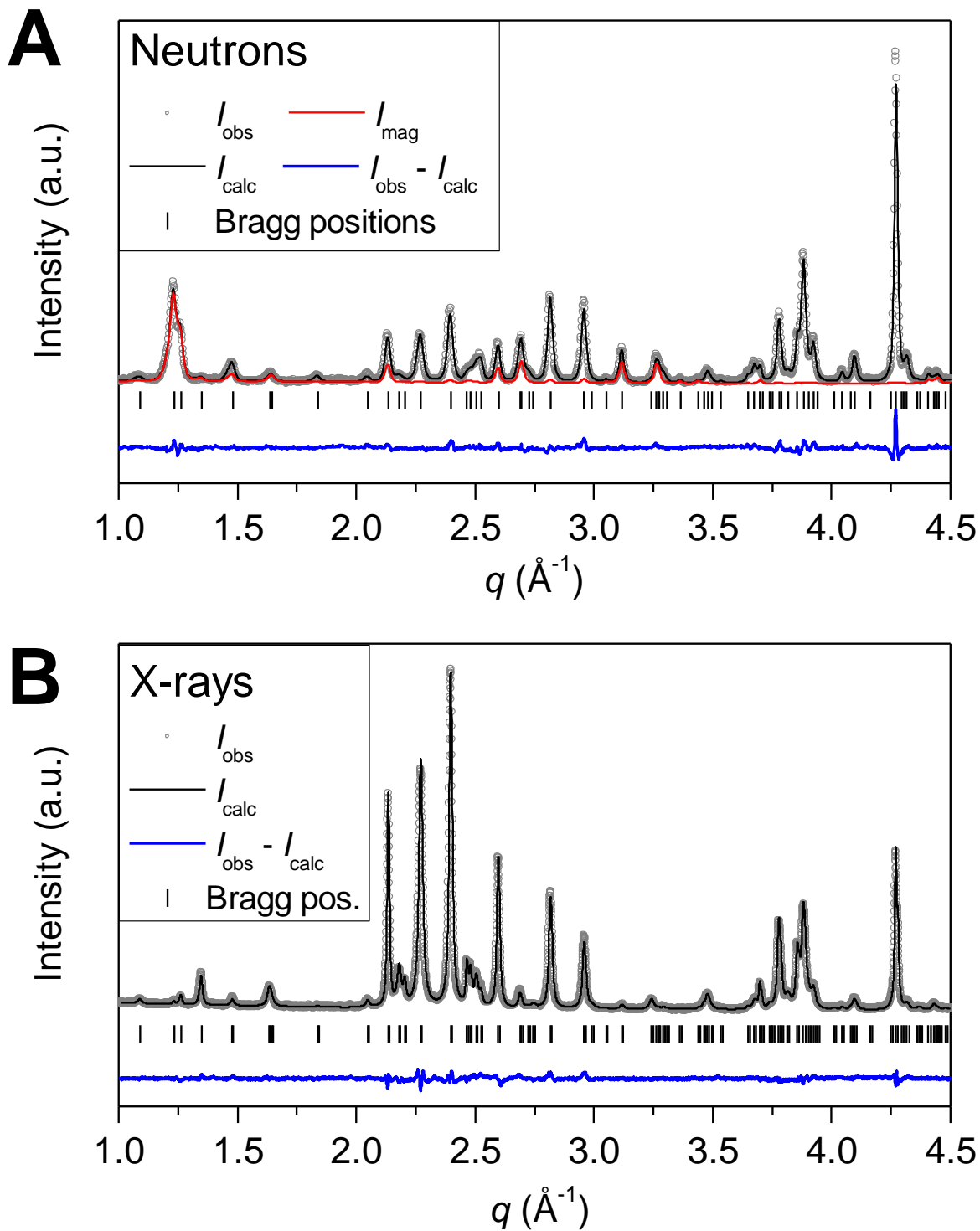


Figure 4: A) NPD and B) PXRD data and constrained Rietveld refinement

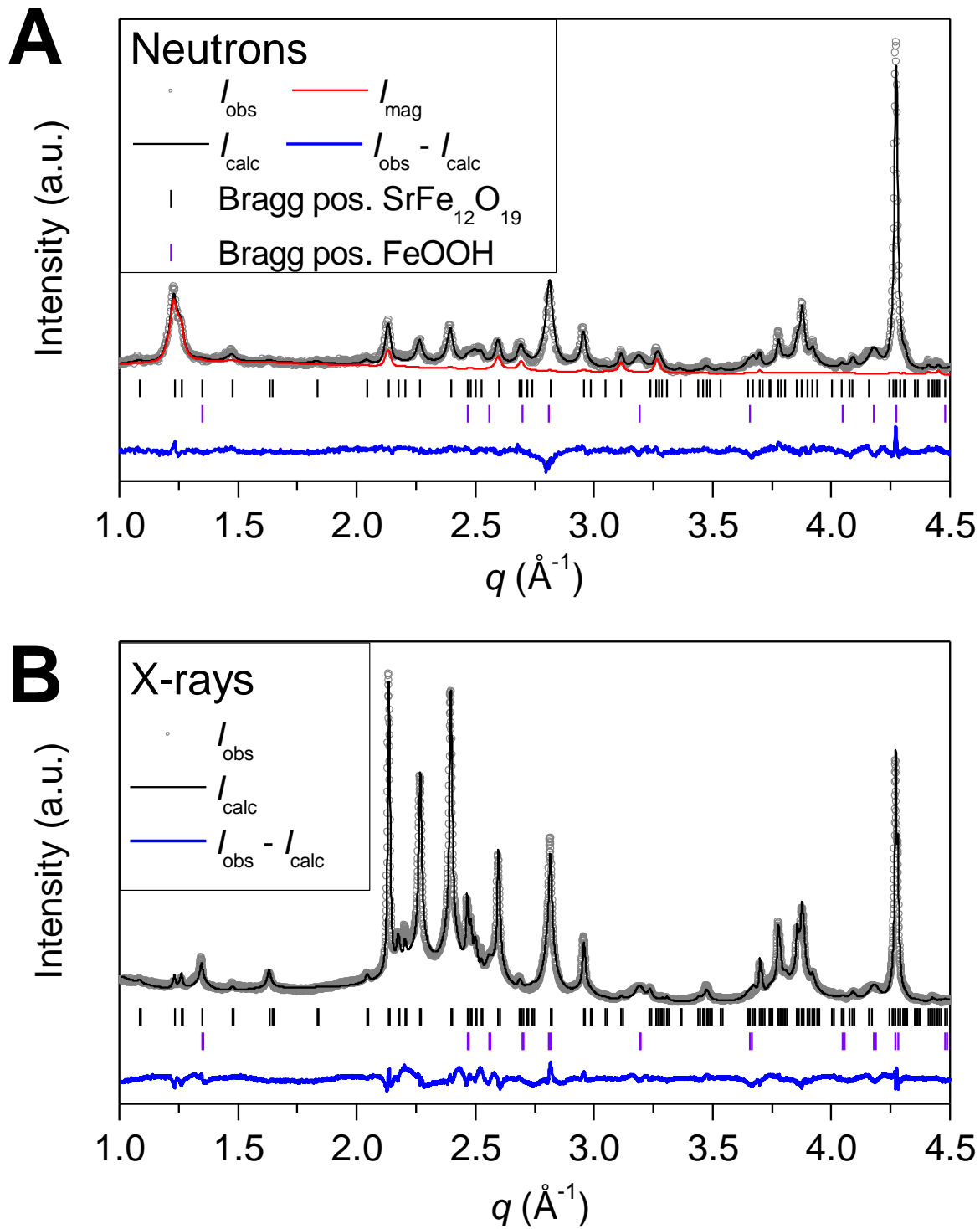


Figure S5: A) NPD and B) PXRD data and constrained Rietveld refinement

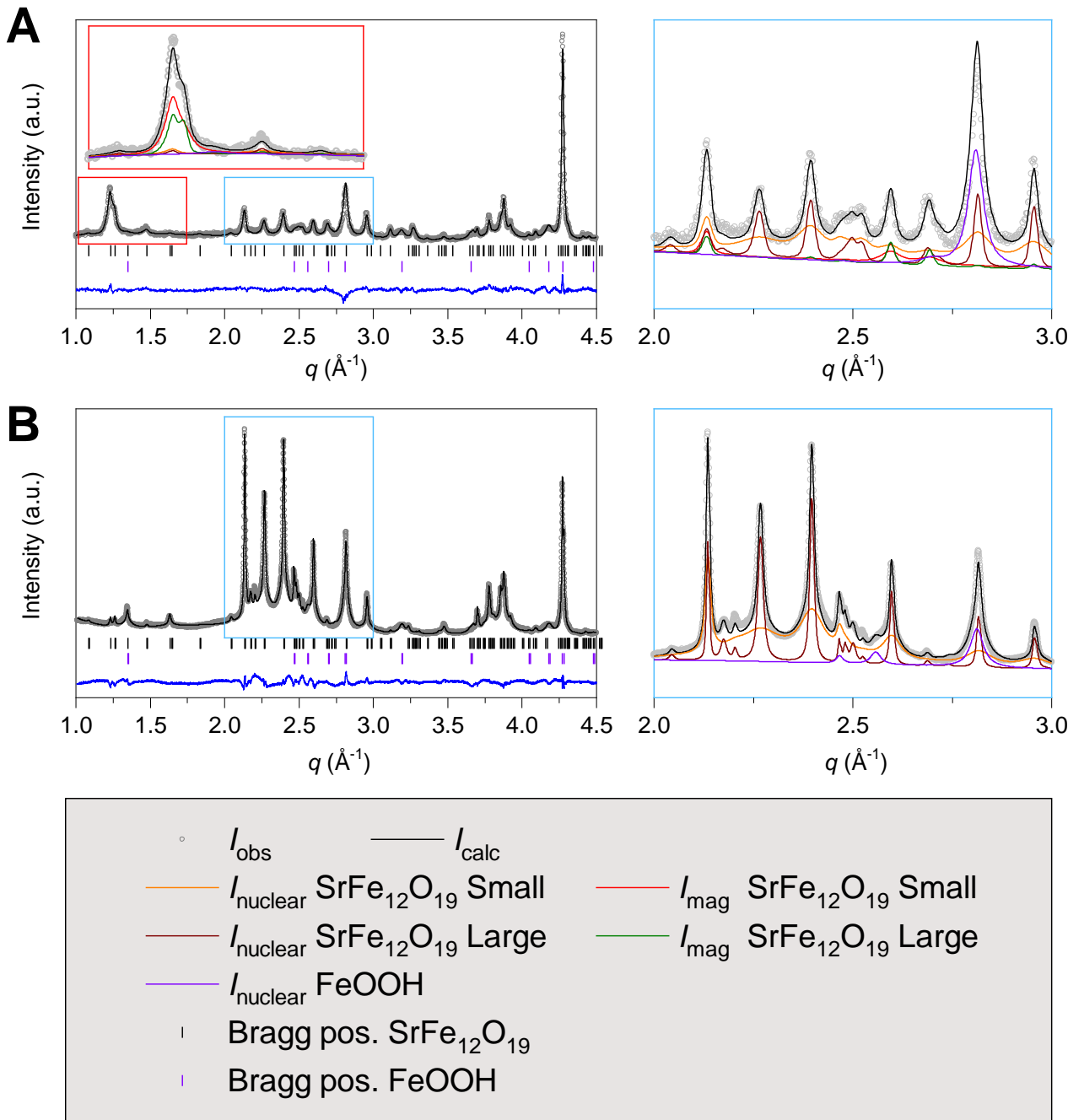


Figure S6: A) NPD and B) PXRD data and constrained Rietveld refinement. Close ups of specific regions of the NPD and PXRD patterns marked with red and blue squares are given, showing all the refined nuclear and magnetic phases of the FL sample.

Autoclave (AC)

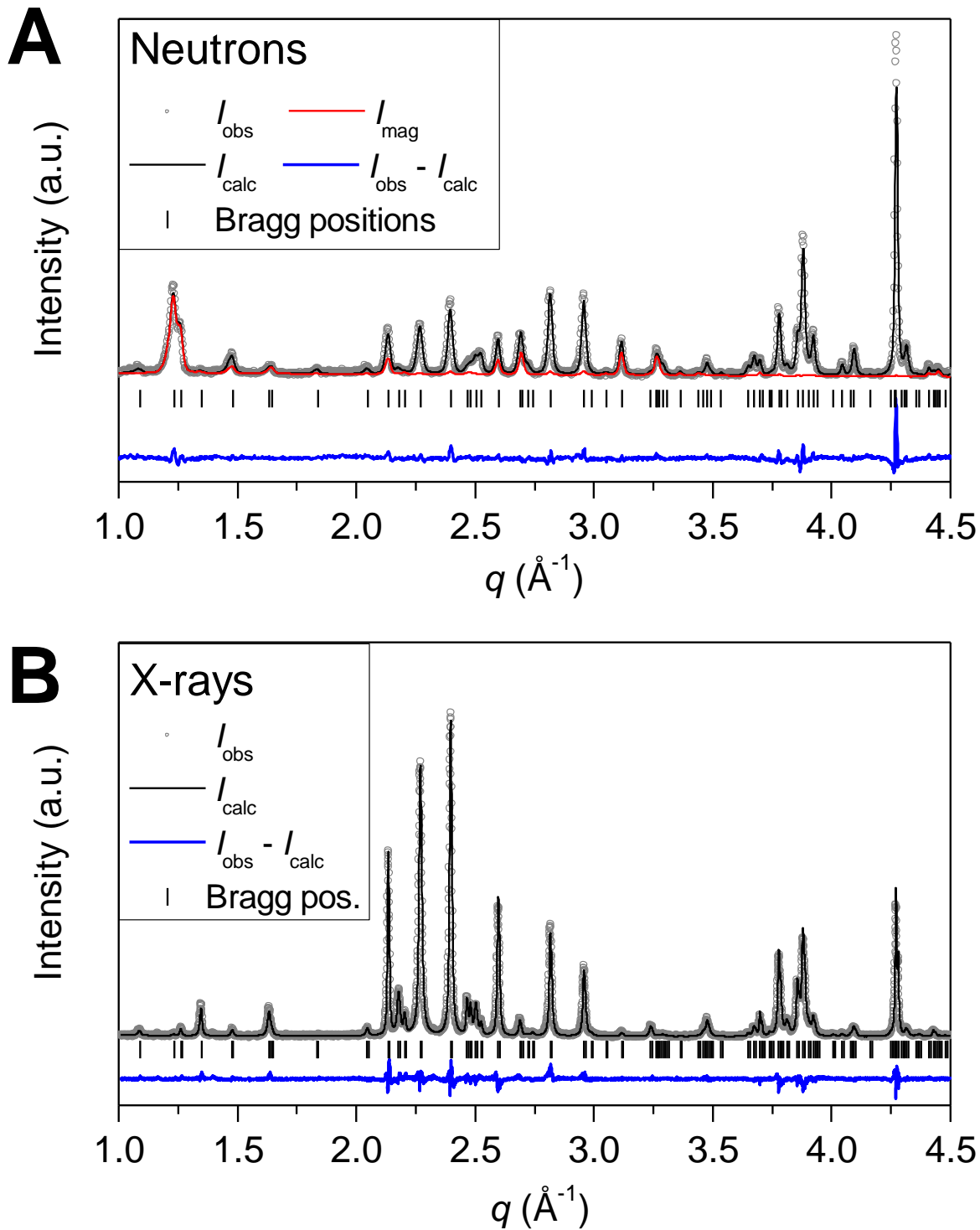


Figure S7: A) NPD and B) PXRD data and constrained Rietveld refinement

Overview of refined structural parameters of SPS samples

Table S2: Extensive summary of the constrained NPD and PXRD refinements including the refined crystal structure and magnetic structure parameters, R-values, etc. (SFO=SrFe₁₂O₁₉)

	SPS_SG		SPS_MSG	SPS_FL		SPS_AC
Phases	SFO	Fe ₃ O ₄	SFO	SFO	α-Fe ₂ O ₃	SFO
Composition and microstructure:						
Wt%, (%)	97.4(4)	2.60(9)	100(2)	99(3)*	1.39(3)*	100(2)
Cryst. size, D _a (nm)	88.3(3)	34.2(5)	163(2)	51.5(1)		240(4)
Cryst. size, D _c (nm)	82(2)	-	106(5)	41.4(6)		130(9)
Crystal structure:						
Space group	P6 ₃ /mmc	Fd-3m	P6 ₃ /mmc	P6 ₃ /mmc	R-3c	P6 ₃ /mmc
Lattice par., a (Å)	5.87814(3)	5.87814(3)	5.87990(3)	5.88069(2)	5.03865(7)	5.88328(3)
Lattice par., c (Å)	23.0623(2)	-	23.0642(2)	23.0705(2)	13.7417(3)	23.0555(2)
Cell vol., V (Å ³)	690.099(8)	591.92(3)	690.572(6)	690.946(7)	302.13(1)	691.104(8)
B _{overall} (PXRD/NPD)	-	-	-	-	-	-
B _{iso} (Sr ²⁺)	0.76(3)	-	0.66(3)	1.09(5)	-	0.78(4)
B _{iso} (Fe ³⁺)	0.22(1)	0.22(1)	0.11(1)	0.45(2)	0.45(2)	0.11(1)
B _{iso} (O ²)	0.22(3)	0.22(3)	0.13(3)	0.32(5)	0.32(5)	0.34(4)
Magnetic structure:						
Easy-axis*	<001>	-	<001>	<001>	-	<001>
μ _{Fe1Oh} (μ _B)	4.4(7)	-	4.2(7)	4.1(9)	-	4.3(7)
μ _{Fe2Oh} (μ _B)	3.4(2)	-	3.3(2)	3.8(3)	-	3.4(2)
μ _{Fe3Oh} (μ _B)	-4.1(3)	-	-4.1(3)	-3.7(4)	-	-4.2(3)
μ _{Fe4td} (μ _B)	-3.5(5)	-	-3.5(4)	-3.9(6)	-	-3.5(4)
μ _{Fe5BP} (μ _B)	3.4(7)	-	3.6(6)	3.6(8)	-	3.5(6)
Fit quality:						
R _{Bragg} (%)	3.53/3.68	5.73/7.60	2.88/4.25	4.34/5.50	5.33/25.0	3.79/4.98
R _F (%)	3.34/2.97	3.86/4.59	2.53/3.11	5.21/3.91	5.83/12.0	3.07/3.27
R _{magnetic} (%)	-/5.34	-	-/5.87	-/4.53	-	-/6.30
χ ² _{global}	25.6		20.0	46.4		26.9
Data						
Wavelength, (Å)	0.49434/2.43870		0.49434/2.43865	0.49434/2.43922		0.49434/2.43928
Background par.	12/6		12/6	14/4		12/6
Ref. param. (total)	54		51	54		50
Data points	4000/3144		4000/3144	4000/3144		4000/3144
Reflect.	772/105	102/15	764/103	784/179	185/21	764/103

*The observed amount and refined weight fractions of SrFe₁₂O₁₉ and α-Fe₂O₃ for this sample differ in the NPD and PXRD patterns (see Figure S10). Whereas no appreciable amount of hematite was observed in the NPD data, a clear presence of this phase was observed in the PXRD pattern. Given that only a fraction of the sample was used for the PXRD measurement, versus the entirety of the sample in the NPD pattern, we believe the NPD results to be more representative of the sample and are therefore the values given in the table. The refined weight fractions from the PXRD pattern were: 88.1(4) wt.% SrFe₁₂O₁₉ and 11.9(1) wt.% α-Fe₂O₃.

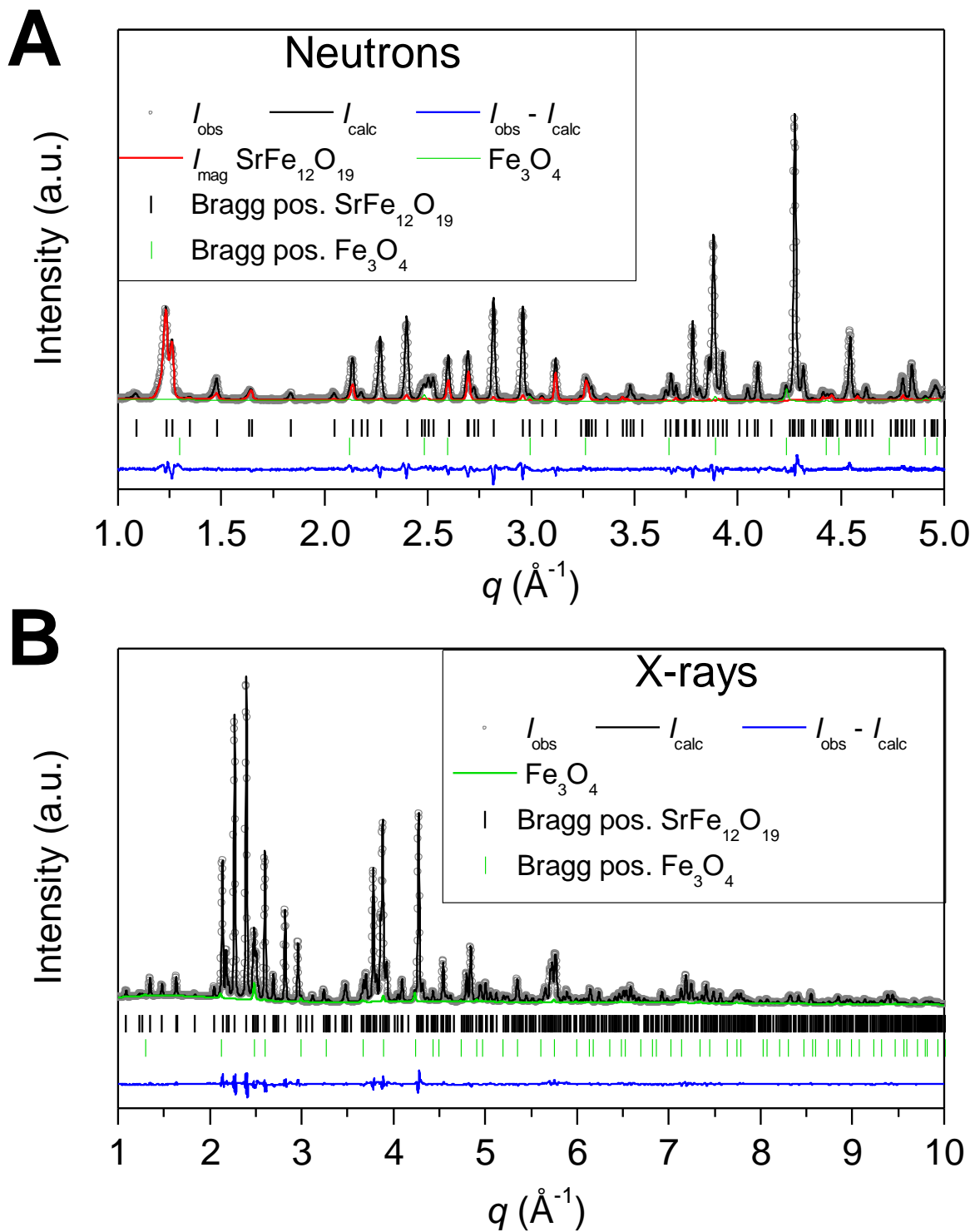


Figure S8: A) NPD and B) PXRD data and constrained Rietveld refinement

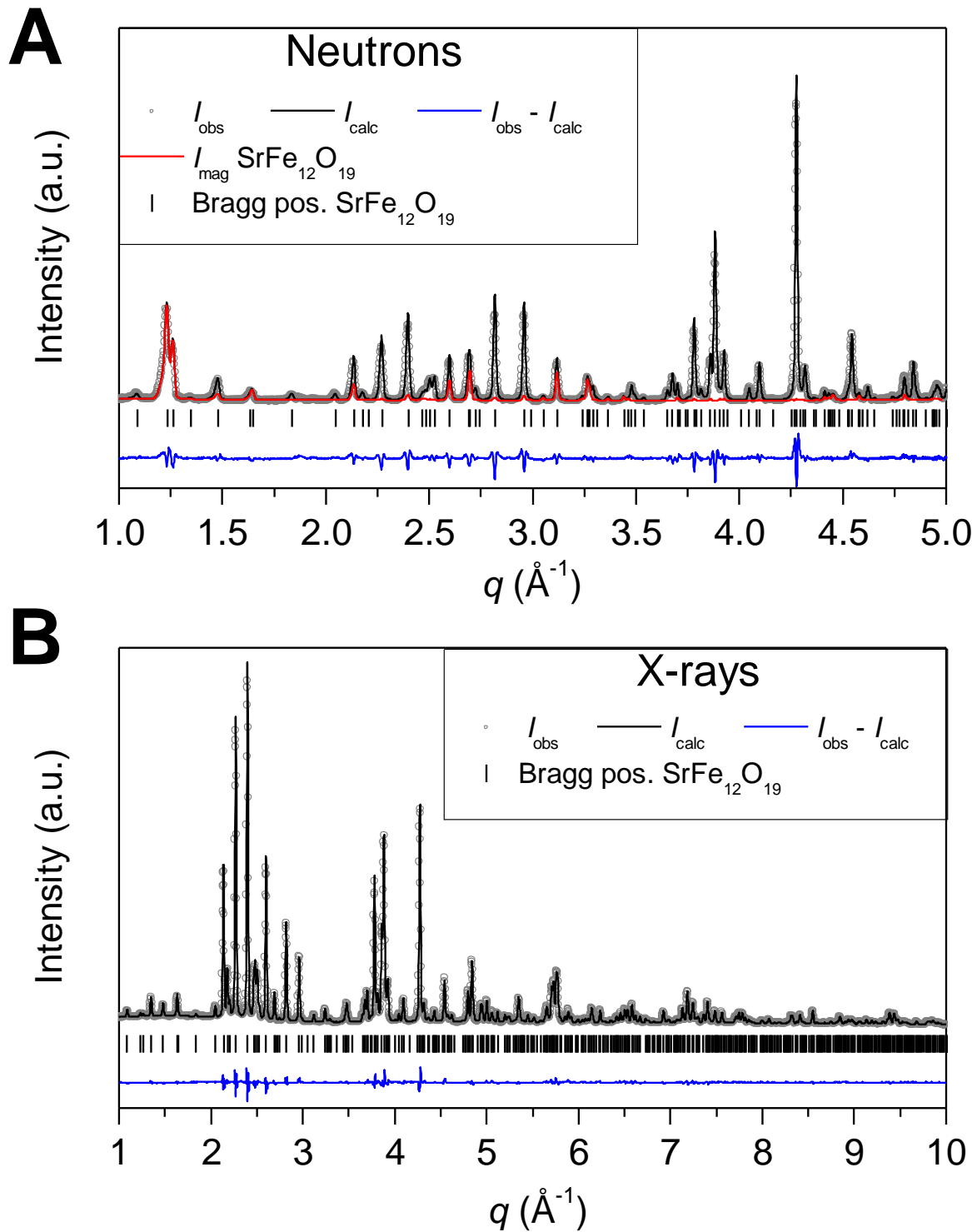


Figure S9: A) NPD and B) PXRD data and constrained Rietveld refinement

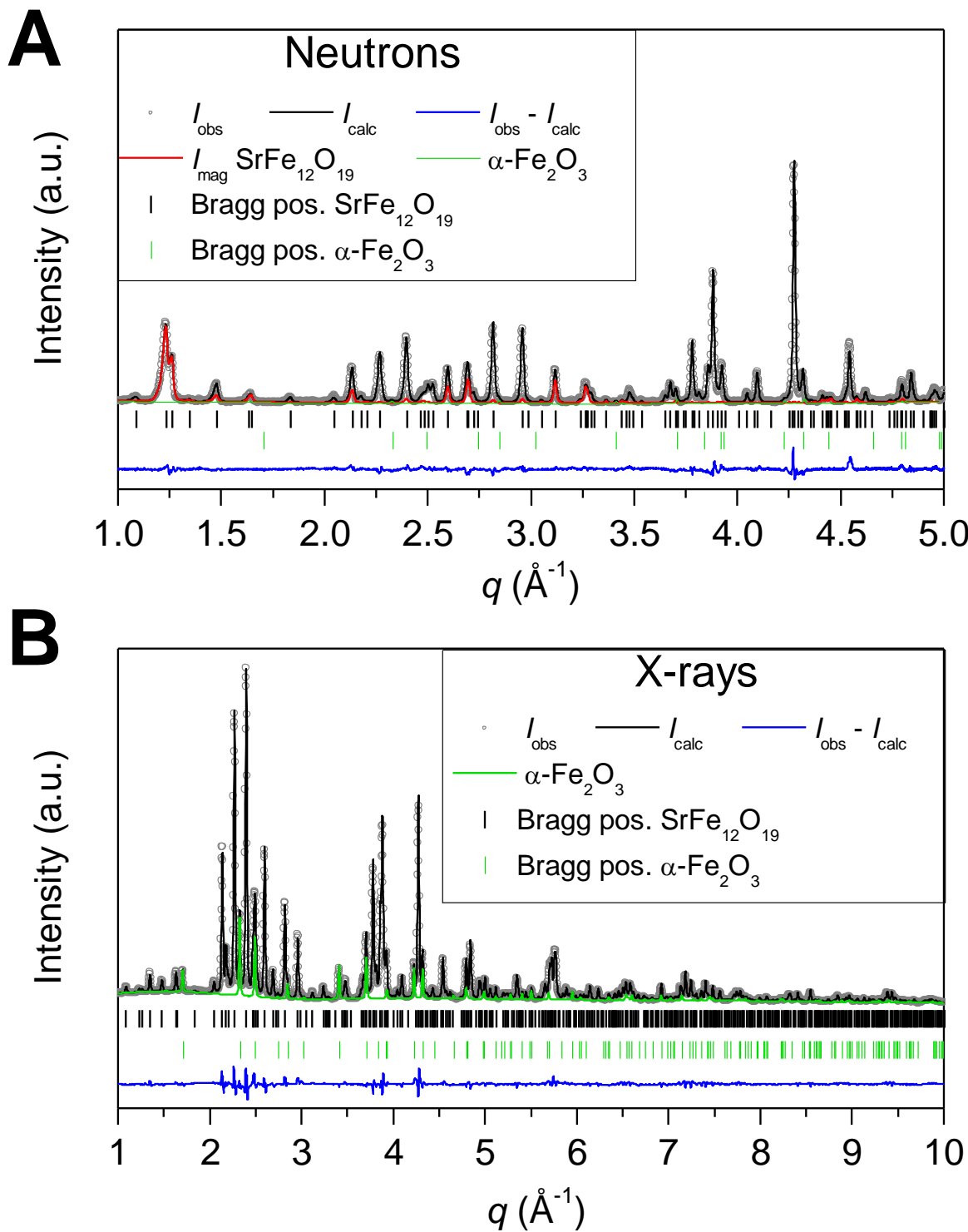


Figure S10: A) NPD and B) PXRD data and constrained Rietveld refinement. While hematite is clearly visible in the PXRD pattern, amounting to 11.9(1) wt.%, no significant amounts of hematite were observed in the NPD data (<2 wt.%). Only a portion of the sample was used to collect PXRD data, whereas the entire sample was used to collect the NPD pattern.

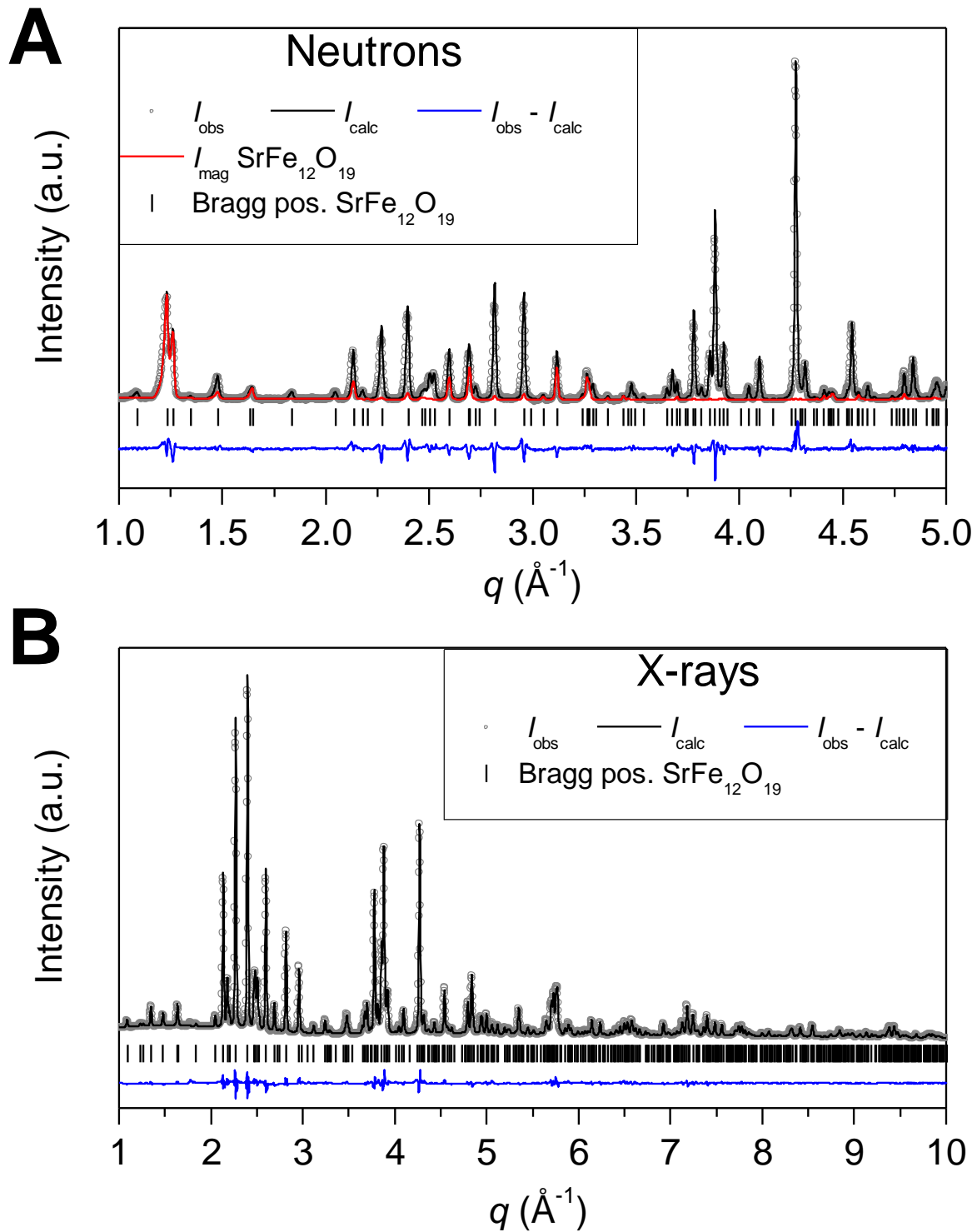


Figure S11: A) NPD and B) PXRD data and constrained Rietveld refinement

Refined magnetic moments

Table S3: Refined magnetic moments of the five different crystallographic sites of Fe^{3+} ions in $\text{SrFe}_{12}\text{O}_{19}$ for the powder and SPS samples

Sample	$\mu_B (\text{Fe1}_{\text{Oh}})$	$\mu_B (\text{Fe2}_{\text{Oh}})$	$\mu_B (\text{Fe3}_{\text{Oh}})$	$\mu_B (\text{Fe4}_{\text{Td}})$	$\mu_B (\text{Fe5}_{\text{BP}})$	$M_{\text{NPD}} (\text{Am}^2/\text{kg})$
SG	3.6(2)	3.00(8)	-3.8(1)	-3.8(1)	3.3(2)	55.1(8)
MSG	3.9(2)	3.34(9)	-3.6(1)	-4.1(2)	2.9(2)	59.2(8)
FL	3.7(7)	3.6(6)	-4.3(3)	-2.4(4)	1.0(7)	69(3)
AC	3.6(2)	3.42(8)	-3.6(1)	-4.2(1)	3.4(2)	62.0(9)
SPS_SG	4.4(7)	3.4(2)	-4.1(3)	-3.5(5)	3.4(7)	65(2)
SPS_MSG	4.2(7)	3.3(2)	-4.1(3)	-3.5(4)	3.6(6)	66(2)
SPS_FL	4.1(9)	3.6(3)	-3.7(4)	-3.9(6)	3.6(8)	74(3)
SPS_AC	4.3(7)	3.4(2)	-4.2(2)	-3.5(4)	3.5(6)	66(2)

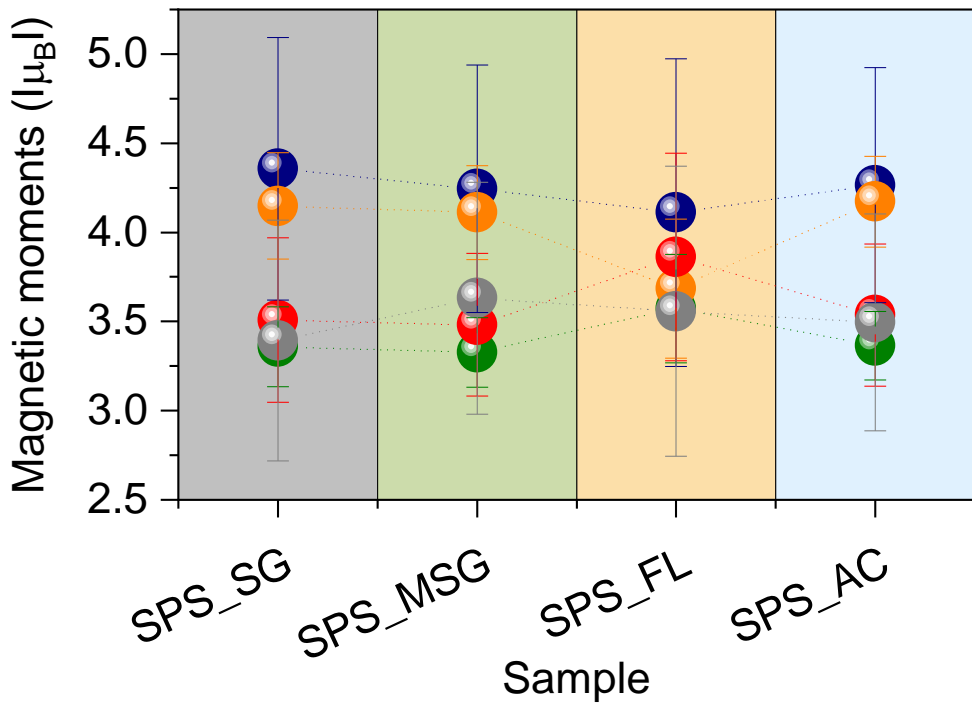


Figure S12: Refined magnetic moments of crushed SPS samples.

Transmission Electron Microscopy

Sol-Gel (SG)

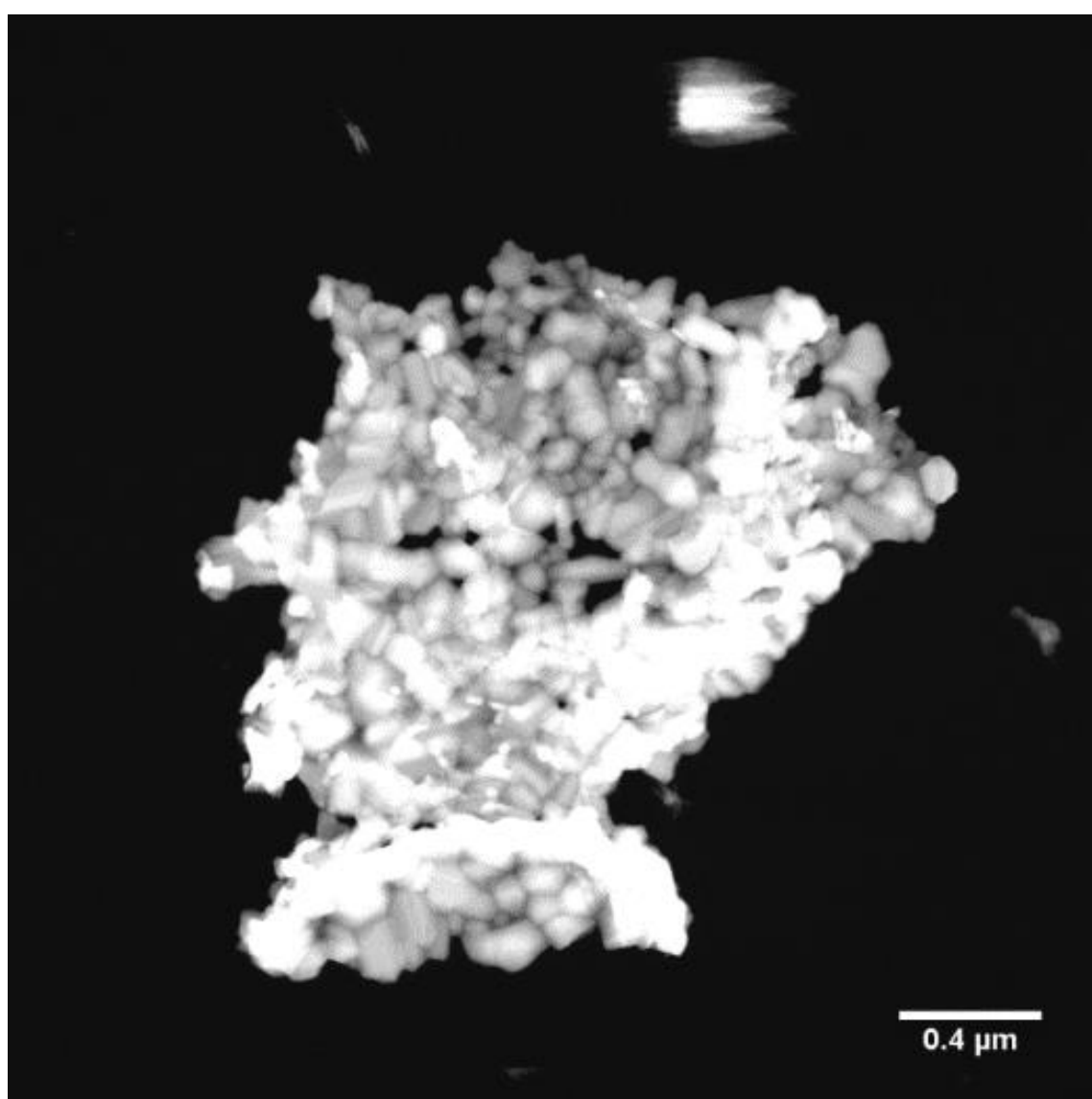


Figure S13: STEM-HAADF micrograph of powders ample SG. The micrograph shows the intergrown nature of the particles, and their lack of defined morphology.

Autoclave (AC)

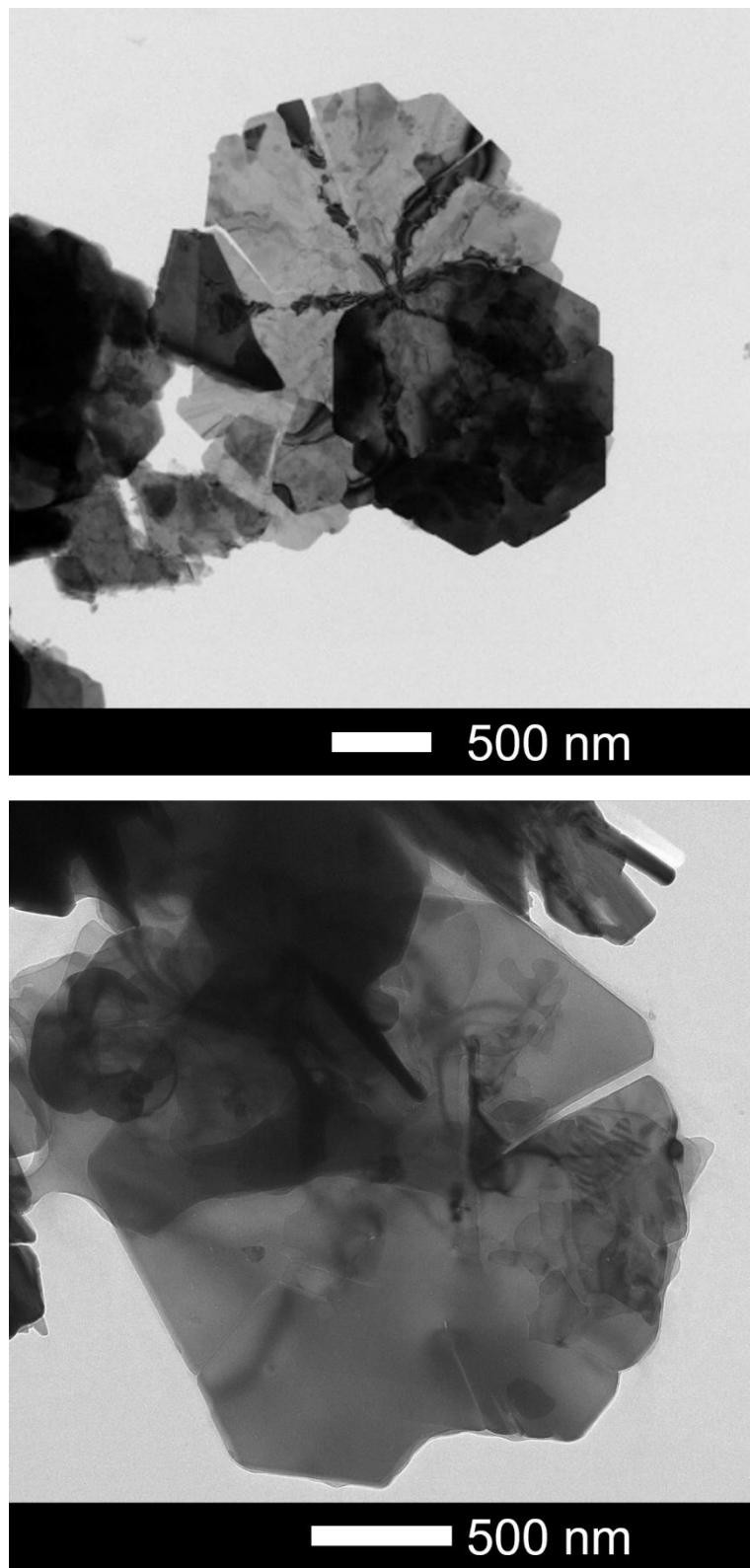


Figure S14: TEM images of sample AC, clearly showing the cracks present on the platelets.

Neutron Pole Figures of SPS samples

SPS_SG

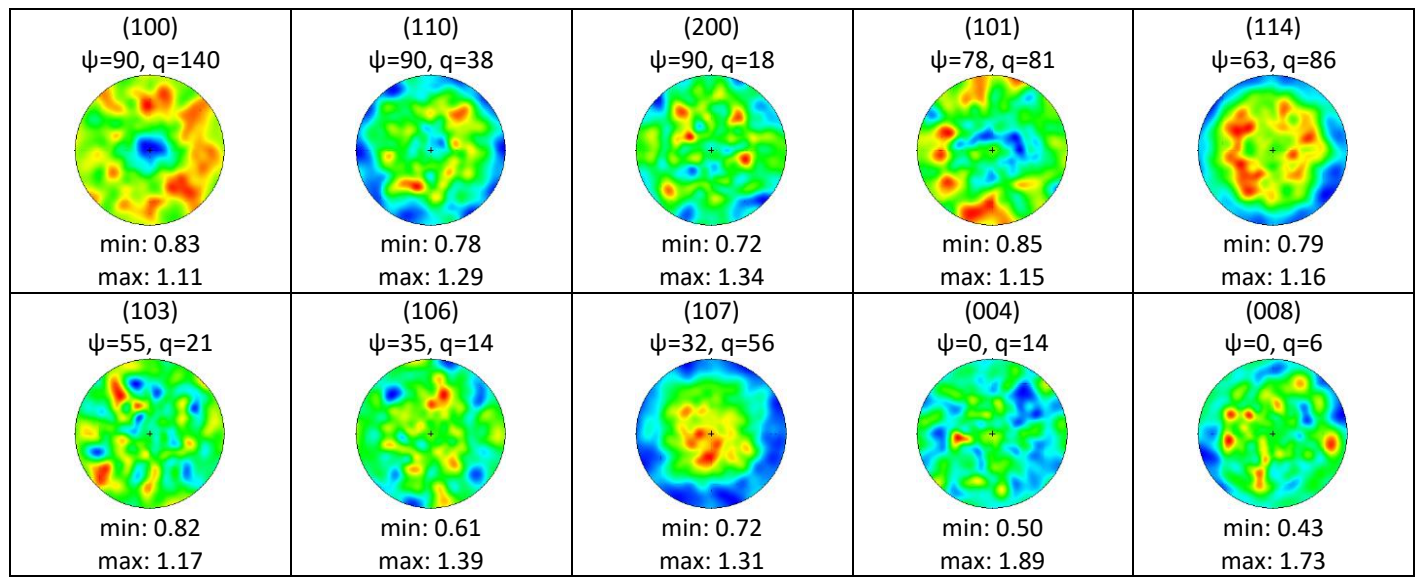


Figure S15: NPFs of sample SPS_SG

SPS_MSG

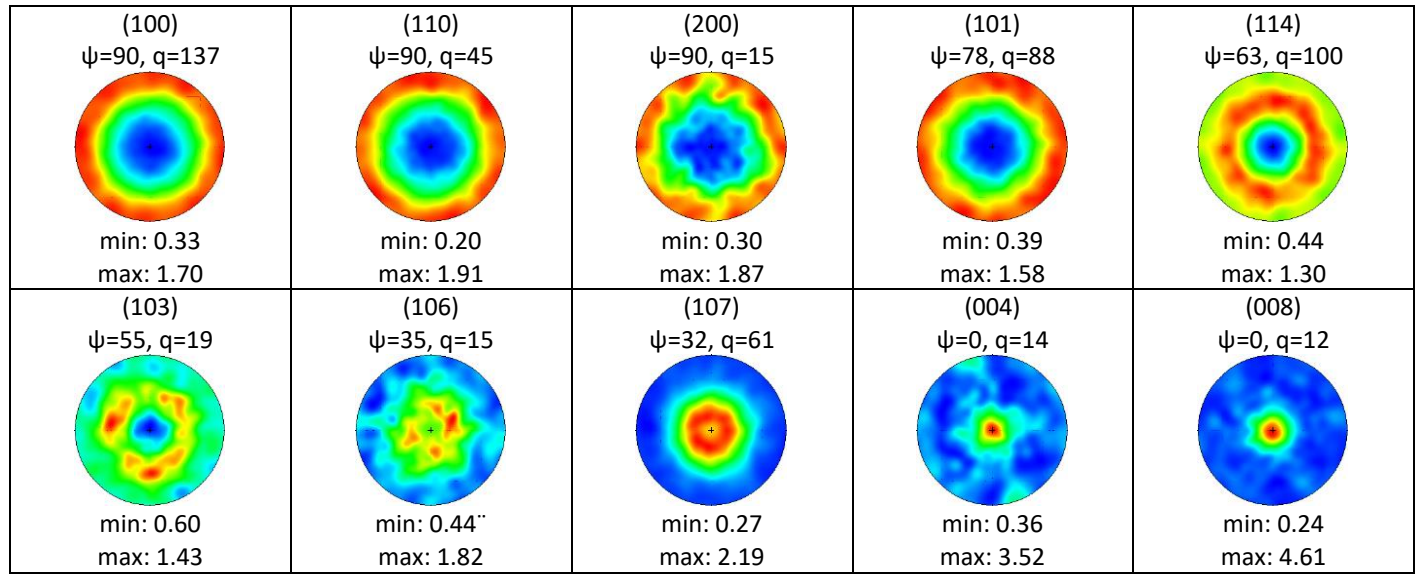


Figure S16: NPFs of sample SPS_MSG

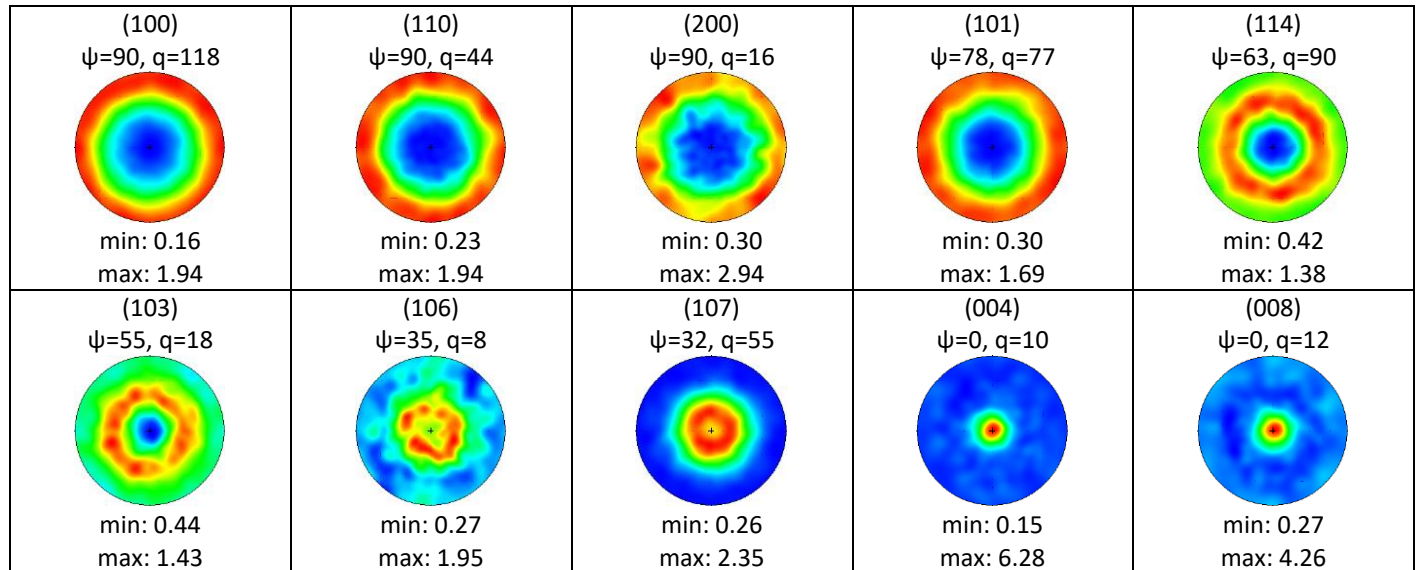
SPS_FL

Figure S17: NPFs of sample SPS_FL

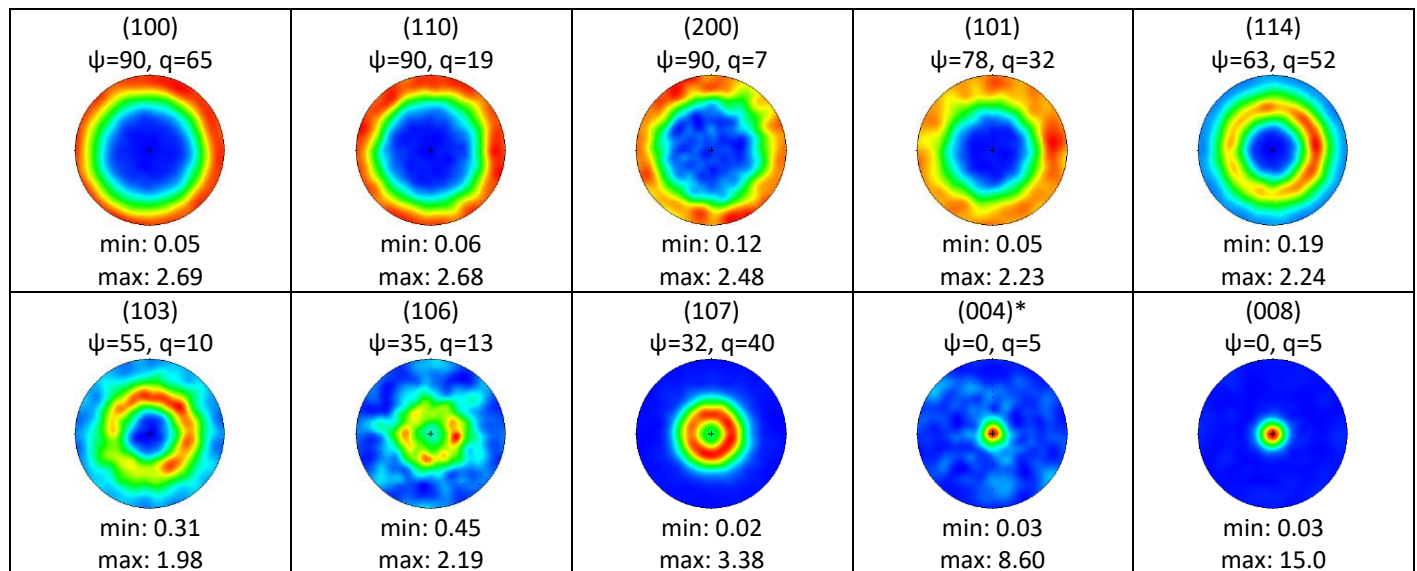
SPS_AC

Figure S18: NPFs of sample SPS_AC

Crystallite growth with SPS

In order to study the crystallite growth with sintering, both the absolute growth along the diameter and the thickness of the platelets, as well as the relative growth with respect to the initial powder crystallites were calculated and plotted in Figure S19. Although no trend is observed in the growth in absolute value between samples, the relative growth is consistently larger along the c -axis of the platelets in all cases. Furthermore, Figure S19B and Figure 2 show that the thinner the initial platelets, the larger the relative growth along the c -axis with sintering. This leads to the observed change in aspect ratio of the post-sintered crystallites compared to the initial powder samples.

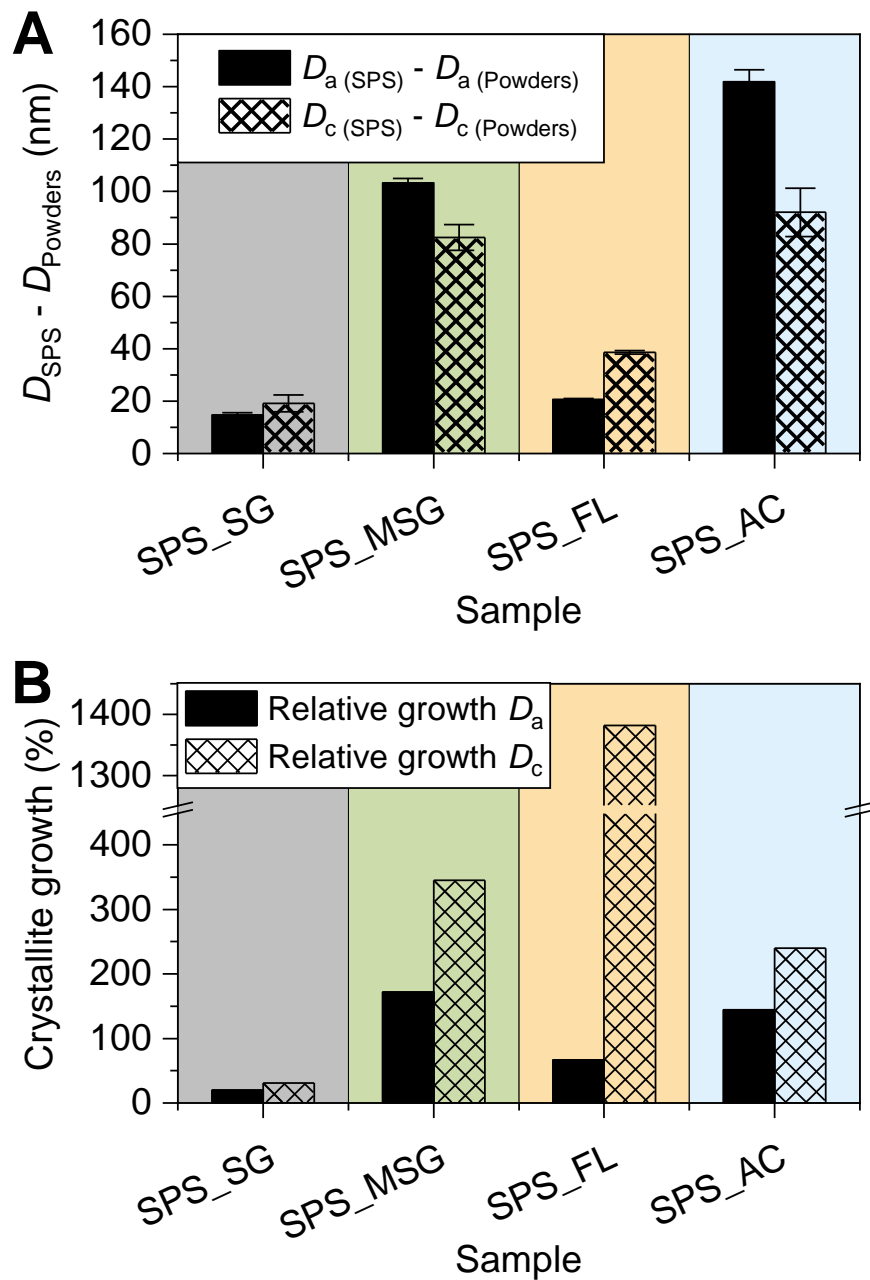


Figure S19: Change in crystallite size between the sintered samples and their powder counterparts. A) Absolute change in size, and B) relative growth along the diameter and thickness of the platelet crystallites.